Computational hints for the simultaneous spectroscopic detection of common contaminants in water

Lina Uribe,[†] Sara Gómez,[*,‡] Franco Egidi,[‡,¶] Tommaso Giovannini,[‡] and Albeiro Restrepo[*,†]

[1]

†*Instituto de Química, Universidad de Antioquia UdeA, Calle 70 No. 52-21, Medellín, Colombia*

‡*Scuola Normale Superiore, Classe di Scienze, Piazza dei Cavalieri 7, 56126, Pisa, Italy*

¶*Current address: Software for Chemistry & Materials BV, De Boelelaan 1083, 1081 HV Amsterdam, The Netherlands*

E-mail: sara.gomezmaya@sns.it; albeiro.restrepo@udea.edu.co

Abstract

In this work, we present a reliable computational methodology with the capability to aid in the identification of ionic water contaminants, such as nitrite, nitrate, and thiocyanate ions, based on the use of Resonance Raman (RR) spectroscopy. The method combines an exhaustive configurational sampling that fully captures the structural complexity inherent to aqueous solutions with state–of–the–art computational techniques that accurately simulate the response properties originating Resonance Raman signals of molecules in solution. Our computational findings show that it is possible to limit the quantum mechanical treatment to only a few explicit water molecules in order to capture the relevant interactions, and thus reproduce the available experimental spectra for NO_2^- and NO_3^-. Once validated, the methodology is applied to the prediction of the RR spectrum of aqueous SCN^-. Our results indicate that by using an incident wavelength of 210 nm, the three emerging contaminants can be simultaneously detected in an aqueous matrix, thus avoiding the laborious indirect measurements used in current protocols. The designed protocol offers generalized explicit benefits: simultaneous detection of pollutants whose absorption spectra overlap, and because of the very nature of RR, pushes detection limits to lower concentrations.

Keywords: UV–Vis, Resonance Raman, nitrite, nitrate, thiocyanate, water contaminants.

1 Introduction

Molecular spectroscopy is a powerful analytical tool for the study of complex chemical systems because of its versatility and its ability to offer direct information about the molecular structure and properties of the analyte.[1,2] The wide variety of available techniques allows for diverse uses which range from the detection of molecules from outer space[3] to the identification of substances which are harmful to humans or other living beings,[4] the latter being particularly relevant for the detection of water contaminants.

Emerging water pollutants can be originated from geogenic or anthropogenic sources, the latter mainly associated with agricultural and industrial activities.[5] In the case of agricultural activities the use of massive amounts of nitrogen-based fertilizers (e.g. nitrate salts) is required for food production.[6] However, only about 40% of the nitrogen content is actually used in the fertilizing process,[7] while the rest usually finds its way to water bodies, resulting in contamination of the water sources for human consumption. The final effect is the creation of huge hypoxic zones around the world due to eutrophication.[8] Biological denitrification,[9] as well as photolysis[10] and photocatalysis[11,12] have been used to remove nitrate (NO_3^-) from water, by reducing it to molecular nitrogen, $N_{2(g)}$. Nevertheless, due to eventual imbalances in the denitrification pathway (for example an insufficient amount of the organic carbon source required by the bacteria during the biological mechanism[9]), the incomplete reduction reaction[10–12] and the excessive use of fertilizers lead to the accumulation of polluting substances in water such as nitrites (NO_2^-). NO_3^- and NO_2^- are both classified by the International Agency for Research on Cancer (IARC)[13] as possible carcinogenic agents for human beings (group 2A in the agency classification) because of their participation in the formation of carcinogenic precursor nitrosamines in the acid environment of the stomach.[14]

Mining and other industrial activities heavily contribute to water contamination with diverse inorganic pollutants, the thiocyanate ion, SCN^-, among them. Even though this molecule is found in different types of foods, high concentrations are harmful and may cause

malfunction of the thyroid gland by acting as a competitive inhibitor to the transport of I^-. SCN^- is thought to reduce the ability of the thyroid to produce the necessary hormones for the proper functioning of the body[15,16] and to catalyze the above mentioned nitrosation reactions involving NO_3^- and NO_2^- leading to the production of nitrosamines.[17]

At this point, it should be clear that aqueous nitrate, nitrite, and thiocyanate play important, mostly noxious roles in human health and that efficient, reliable and robust protocols are needed for rapid assessment of their presence in complex samples. Regrettably, that is not the case because there are no current standard methods to simultaneously identify all three ions in aqueous samples, on the contrary, detection of multiple contaminants and quantification in water by spectroscopic techniques requires a series of laborious indirect procedures and measurements summarized next. Internationally accepted colorimetric methodologies are used to detect and quantify NO_2^- by diazotizing it with sulfanilamide and subsequent coupling with N–(1–naphthyl)–ethylenediamine dihydrochloride leading to the formation of a reddish purple azo dye which absorbs at 540 nm.[18] NO_3^- is quantitatively reduced to NO_2^- (e.g. by hydrazine or cadmium reduction methods) and both the original and resulting nitrite are determined by the aforementioned diazotizing reaction.[18] Quantification of SCN^- in water is carried out through a complexation reaction with Fe^{3+} ions to form a colored species ($[FeSCN]^{2+}$) that absorbs at 460 nm.[19]

Vibrational spectroscopies have also been used with the purpose of identifying and quantifying these ions in aqueous matrices. By means of conventional (also known as spontaneous) Raman spectroscopy, nitrite and nitrate have been unequivocally detected,[20–25] however, several analytic studies have shown that Resonance Raman (RR) spectroscopy provides even lower detection limits, as listed in Table 1. Both spontaneous and resonance Raman are named after the Raman effect of inelastic scattering of light, however, in RR, the incident wavelengths are in resonance with electronic transitions,[26] resulting in selective enhancement of the spectroscopic responses between 3 and 6 orders of magnitude when compared against conventional Raman.[27] The selective amplification of spectroscopic responses suggests RR

as an analytical technique with the potential to help in the simultaneous detection of pollutants in very dilute solutions. In fact, not only have Ianoul et al.[28] proposed the use of RR spectroscopy as a direct tool to simultaneously monitor nitrite and nitrate in wastewater treatment processes, but, in 2005, the United States Environmental Protection Agency announced the development of deep UVRR equipment for the same purposes.[29]

Table 1: Experimental Limits of Detection (LOD) for nitrite and nitrate ions in water samples. ω_0 denotes the laser wavelength used for the detection.

Source	**Ion**	ω_0 **(nm)**	**Technique**	**LOD**
Lombardi et al.[20]	NO_2^-	514.5	Raman	14.4 mM (206 ppm)
Ahmadjian and Brown[21]	NO_3^-	488 and 514.5	Raman	150 ppm
Baldwin and Brown[22]	NO_3^-	488 and 514.5	Raman	25 ppm
Cunningham et al.[23]	NO_3^-	488	Raman	9.79 ppm
Furuya et al.[24]	NO_3^-	488	Raman	2 ppm
Gajaraj et al.[25]	NO_3^- NO_2^-	785	SERS	0.5 ppm No reported
Ianoul et al.[28]	NO_3^- NO_2^-	229	RR	< 14 μM (200 ppb)

UVRR is a complex phenomenon which arises from the coupling of both electronic and vibrational degrees of freedom to an external electromagnetic radiation, therefore the resulting spectra are often difficult to analyze and rationalize, thus, computational simulations provide invaluable assistance. However, successful combination of experiments and calculations mandate that the reliability of computational models has to be fully demonstrated. Alas, the complexity of the phenomenon is further exacerbated by the fact that most analytes are detected in solution with the solvation environment heavily influencing the spectroscopic response, therefore, specific solvent effects have to be accurately taken into account in the simulations. Accordingly, for the study of spectroscopic properties of systems in aqueous solution, a wide variety of methods have been proposed and tested.[30,31] One of the most difficult problems that must be addressed in the development of computational methods to describe dilute analytes is the fact that those systems cannot be represented by a single minimum energy structure, rather, ensembles of many different solute–solvent and solvent–solvent

configurations, each with its own spectroscopic properties, are needed. In this context, the generation and identification of meaningful microstates (structures with high probability of existence) for solvated systems is a problematic issue, exacerbated by the fact that the number of stationary points within a given Potential Energy Surface (PES) increases exponentially with size. Molecular Dynamics (MD), Simulated Annealing (SA), and a variety of stochastic sampling strategies are commonly used for the exploration of complex PESs proper of solutes surrounded by water molecules. As a matter of fact, MD and SA methodologies have been used in recent works for microsolvated nitrite and nitrate,[32,33] affording molecular clusters that perfectly reproduce experimental structural and energetic data and therefore are instrumental in the interpretation of UV–Vis and IR experimental features.

We develop here a computational methodology that accurately determines the Resonance Raman spectra of ions in aqueous solutions. With that protocol, we show that there exist potential incident wavelengths to be used in RR experiments to simultaneously identify and quantify ions in very dilute solutions, which will serve as a preliminary step to guide experimental setups free of unnecessary complications and indirect measurements. NO_3^-, NO_2^-, and SCN^- ions were chosen as study cases, because of their importance as water contaminants. Nitrate and nitrite ions are ideal to validate the methodology since there is ample experimental data to compare the computed results. Once validated, the protocol is employed to predict the RR spectra of both, solvated thiocyanate, and a mixture of the three ions in more complex aqueous matrices. The outline of the paper is as follows. In section 2, we describe computational methods for the configurational sampling and for the calculation of the UV–Vis and RR spectra. In section 3, the simulated spectra are discussed and compared against experimental data when possible. Finally, in section 4 the main outcomes of the study are summarized.

2 Computational Methods

2.1 Configurational sampling

It is well established that in order to reproduce experimental spectroscopic results, exhaustive samplings of the configurational spaces of the systems of interest is mandatory, and for the microsolvated environments one must take into account not only the putative global minima, but all clusters having meaningful probabilities of existence.[32–38] To tackle the problem of the configurational sampling in the chosen systems, namely, solvated nitrite, nitrate, and thiocyanate, and to recover the most representative motifs within the corresponding PES for microsolvation, the ASCEC (Spanish acronym for Annealing Simulado Con Energía Cuántica) algorithm[39,40] was used. The ASCEC program[41] is an application of the SA algorithm, where the energy of each randomly generated configuration along a Markov chain is evaluated quantum mechanically and then kept or not as candidate for a stationary point after passing/failing a modified Metropolis acceptance test.[42] See Refs. 39,40 for detailed discussion of the ASCEC algorithm.

Under the annealing conditions listed in Table S1, ASCEC afforded candidate structures for $[\mathrm{SCN}\,(\mathrm{H_2O})_x]^-$ with $x = 1-6$, which were optimized at the B3LYP/6–311++G(d,p) level of theory. In a previous work,[32] we demonstrated that five explicit water molecules combined with the Polarizable Continuum Model (PCM) (ASCEC sampling + PCM method) are enough to recover all features of the UV–Vis experimental spectrum of nitrite in aqueous solution, whereas for nitrate the same number of solvent molecules provided a very good representation of the IR spectrum.[33] The need for explicit solvent molecules is justified on the basis that the orbitals involved in the main transitions belong not just to the solute but also to the nearest water molecules, which are often bound via hydrogen bonds. Then, for the $[\mathrm{NO_3}\,(\mathrm{H_2O})_5]^-$ and $[\mathrm{NO_2}\,(\mathrm{H_2O})_5]^-$ cases, we borrowed the reported structures,[32,33] which were obtained with the same sampling method. Therefore, to calculate te spectra we

used the 68 and 26 clusters found for nitrite and nitrate respectively, with a cluster size of five waters. For consistency, the reported motifs for $[NO_3\,(H_2O)_5]^-$ were reoptimized at the same model chemistry used for nitrite and thiocyanate.

2.2 Calculation of spectra

Once optimized and classified, the clusters obtained with ASCEC were used in the following spectroscopy calculations, using as weighting factors cluster populations derived from Boltzmann distributions of the Gibbs free energies of formation.

2.2.1 UV–Vis absorption spectra

A necessary prerequisite to obtain a RR spectrum is to determine the wavelengths at which electronic transitions take place, to this end, absorption spectra for the microsolvated ions were calculated using TD–DFT,[43–46] converging the first 12 excited states. Preliminary tests indicated that for nitrite and nitrate a lower number of states can be used without affecting the quality of the simulated spectra, i.e., the first seven and five singlet excited states respectively. For all the systems, the UV–Vis absorption spectra were convoluted with a Gaussian lineshape with a Full Width at the Half Maximum (FWHM) of 0.4 eV.

2.2.2 Resonance Raman spectra

RR spectra were simulated by using the Franck–Condon Vertical Gradient (FC|VG) approximation, where the excited state gradients are calculated at the ground state equilibrium geometries. The procedure was adapted from Refs. 27,47, where it was found to provide excellent agreement between computed and experimental data. Here we simply summarize the equations of the invariants a, δ, γ (Eq. 1), where $\left(\tilde{\alpha}_{\alpha\beta}\right)_{mn}$ are the corresponding Cartesian components of the complex electric dipole–electric dipole transition polarizability Raman

tensor for the initial and final molecular states $|n\rangle$ and $|m\rangle$, respectively.

$$a^2 = \frac{1}{9}\mathrm{Re}\Big[\big(\tilde{\alpha}^s_{\alpha\alpha}\big)_{mn}\big(\tilde{\alpha}^{s*}_{\beta\beta}\big)_{mn}\Big] \tag{1a}$$

$$\delta^2 = \frac{3}{2}\mathrm{Re}\Big[\big(\tilde{\alpha}^a_{\alpha\beta}\big)_{mn}\big(\tilde{\alpha}^{a*}_{\alpha\beta}\big)_{mn}\Big] \tag{1b}$$

$$\gamma^2 = \frac{1}{2}\mathrm{Re}\Big[3\big(\tilde{\alpha}^s_{\alpha\beta}\big)_{mn}\big(\tilde{\alpha}^{s*}_{\alpha\beta}\big)_{mn} - \big(\tilde{\alpha}^s_{\alpha\alpha}\big)_{mn}\big(\tilde{\alpha}^{s*}_{\beta\beta}\big)_{mn}\Big] \tag{1c}$$

$$\big(\tilde{\alpha}_{\alpha\beta}\big)^s_{mn} = \frac{1}{2}\Big[\big(\tilde{\alpha}_{\alpha\beta}\big)_{mn} + \big(\tilde{\alpha}_{\beta\alpha}\big)_{mn}\Big] \tag{2a}$$

$$\big(\tilde{\alpha}_{\alpha\beta}\big)^a_{mn} = \frac{1}{2}\Big[\big(\tilde{\alpha}_{\alpha\beta}\big)_{mn} - \big(\tilde{\alpha}_{\beta\alpha}\big)_{mn}\Big] \tag{2b}$$

The superscripts s and a refer to purely symmetric and antisymmetric parts (Eq. 2).[48] RR intensities are then formulated in terms of the previous invariants, depending on the illumination–observation geometry and the experimental setup.[49,50] For an incident linear polarized radiation $\perp^i$, in an observation angle of $\frac{\pi}{2}$ and with a total scattered radiation, $\|^s + \perp^s$, the cross–section is given by Eq. 3, where ω_s is the magnitude of the angular frequency associated with the vibrational transition from $|n\rangle$ to $|m\rangle$.

$$\sigma'\big(\frac{\pi}{2}, \|^s + \perp^s, \perp^i\big) = \frac{\omega_s^4}{c^4}\frac{45a^2 + 7\delta^2 + 5\gamma^2}{45} \tag{3}$$

The contribution from different selected electronic states was added at the amplitude (polarizability) level and RR stick spectra were convoluted with Lorentzian functions with an FWHM value of 20 cm^{-1}. For the most important normal modes we track how the RR intensities change by varying the incident wavelength ω_0. To this end, we build Resonance Raman Excitation Profiles (RREP) with ω_0 ranging from 160 nm to 400 nm.

For the sake of comparison, off–resonance Raman spectra were also computed for the same clusters. Raw and convoluted (Lorentzian functions, with an FWHM of 8 cm^{-1}) data calculated at 532 and 1064 nm are depicted in Figures S12, S13 of the Electronic Supplementary Information (ESI). All calculations were performed using the Gaussian16 program.[51]

3 Results and discussion

In this section we first analyze the structural and energetic aspects of the microsolvated nitrite, nitrate and thiocyanate. Next, we discuss their UV–Vis spectra examining the transitions involved and then, for each case, we focus on the Resonance Raman spectral signals. We compare our results against experimental data (when available) and based on the quality of our approach, the RR spectra of thiocyanate and of a mixture of the three ions in water are predicted.

3.1 Structures

3.1.1 Nitrite and Nitrate

The structural problem for nitrate and nitrite clusters with five explicit water molecules was previously solved,[32,33] in Figure 1 the structures of the global minima are displayed together with their Gibbs free energy based Boltzmann populations. These representative clusters encompass the largest probabilities of existence at standard conditions and thus will be the major contributors to any calculated or measured property, spectral signals among them, however, since their populations are not near 100%, contributions from other meaningful isomers must be statistically weighted by their Boltzmann distributions.

Nitrite	Nitrate	Thiocyanate	
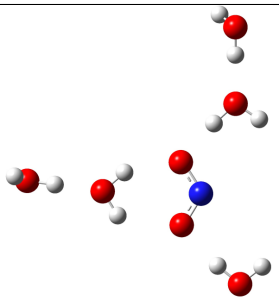	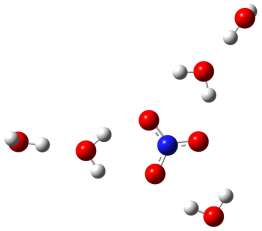	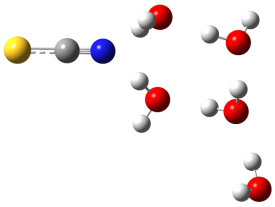	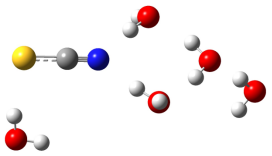
W_5S_1; ΔE_G= 0.00	W_5S_1; ΔE_G= 0.00	W_5S_1; ΔE_G= 0.00	W_5S_2; ΔE_G= 0.27
$\%\chi_i G$ = 68.7	$\%\chi_i G$ = 56.3	$\%\chi_i G$ = 36.8	$\%\chi_i G$ = 23.3

Figure 1: Structures of the lowest energy $[NO_2\,(H_2O)_5]^-$, $[NO_3\,(H_2O)_5]^-$ and $[SCN\,(H_2O)_5]^-$ clusters optimized at the B3LYP/6–311++G(d,p) level with their respective isomer populations ($\%\chi_i$G) derived from the Boltzmann distribution of the Gibbs energies.

3.1.2 Thiocyanate

Table 2 lists the total number of isomers obtained by sampling the PES of the $[SCN\,(H_2O)_x]^-$ clusters with $x = 1-6$. A total of 305 equilibrium structures were found with binding energies ranging from -12.09 to -61.82 kcal/mol. The entire set of structures is available in Figures S1, S2, S3, S4, S5 and S6 (Cartesian coordinates are also included in the ESI). We point out that in all cases, binding energies are very close to those reported for the microsolvation of nitrite and nitrate (see Table S2) but are considerably larger than for pure water clusters of similar molecularities,[40,52–54] with the additional stabilization clearly coming from the presence of the formal negative charge. The small energy differences among isomers belonging to the same PES listed in Table 2 and the corresponding isomer populations (see below), reflect, with the same argumentation as for NO_2^- and NO_3^-, that several $[SCN\,(H_2O)_x]^-$ structures actually contribute to the computed spectra. Also, similar to nitrite and other anion cases, at this low molecularities, the stabilization of thiocyanate tends to increase with the number of water molecules.

In previous studies, the hydration structures of SCN^- have been explored using molecular dynamics,[55] stochastic methods,[56] or simply replacing water molecules with the thiocyanate ion in selected pristine water clusters.[57] In the context of this work, it is important to notice

Table 2: Structural complexity of the B3LYP/6–311++G(d,p) potential energy surfaces for the microsolvation of SCN^- with up to six water molecules. All minima are within ΔE, ΔE_H and ΔE_G of the corresponding global minimum. ΔE_H and ΔE_G at 298.15 K, 1 atm. Energy values are given in kcal/mol.

x	Number of isomers	ΔE	ΔE_H	ΔE_G
1	6	4.40	3.87	5.55
2	40	5.13	4.97	6.36
3	60	6.71	6.86	7.83
4	62	5.95	7.27	6.86
5	63	13.23	12.99	16.20
6	74	29.23	30.23	28.03

that the ASCEC sampling and further optimization of candidate structures affords the most comprehensive picture to date of cluster structures involved in the microsolvation of SCN^- with up to six water molecules, that is, our sampling technique recovers all structures previously reported and finds new meaningful isomers. The two lowest Gibbs energy structures for clusters with five waters are shown in Figure 1 alongside the putative global minima for $[NO_2\,(H_2O)_5]^-$ and $[NO_3\,(H_2O)_5]^-$. It is worth noticing that in the majority of cases, and predominantly for the global minima, the structures present an asymmetric hydration shell, where the water molecules form H–bonds preferentially with the nitrogen atom. This behavior has been already experimentally observed when aqueous solutions of KSCN were studied with neutron diffraction.[58,59] The placement of solvent molecules around the sulphur end of thiocyanate is also in line with the classification of this ion as a chaotrope ("structure breaker and weakly hydrated anion") in the Hofmeister series.[60]

3.2 UV–Vis spectroscopy

It is well known[61–63] that the maxima of the UV–Vis electronic absorption spectra of the three aqueous ions overlap in the spectral region from 200 to 240 nm (see Figure 2 (a)). This fact prevents their simultaneous detection by this particular technique. Our simulated spectra (see Figure 2 (b)) for the Boltzmann averaged $[NO_2\,(H_2O)_5]^-$, $[NO_3\,(H_2O)_5]^-$ and $[SCN\,(H_2O)_5]^-$ clusters exhibit the same behavior, thus validating the computational

methodology (i.e. both the solvation approach and the chosen level of theory). Conversely, large discrepancies with experiments are found when the continuum solvation approach, PCM, is used without explicit water molecules to simulate the spectra (see Figure S7 in the ESI).

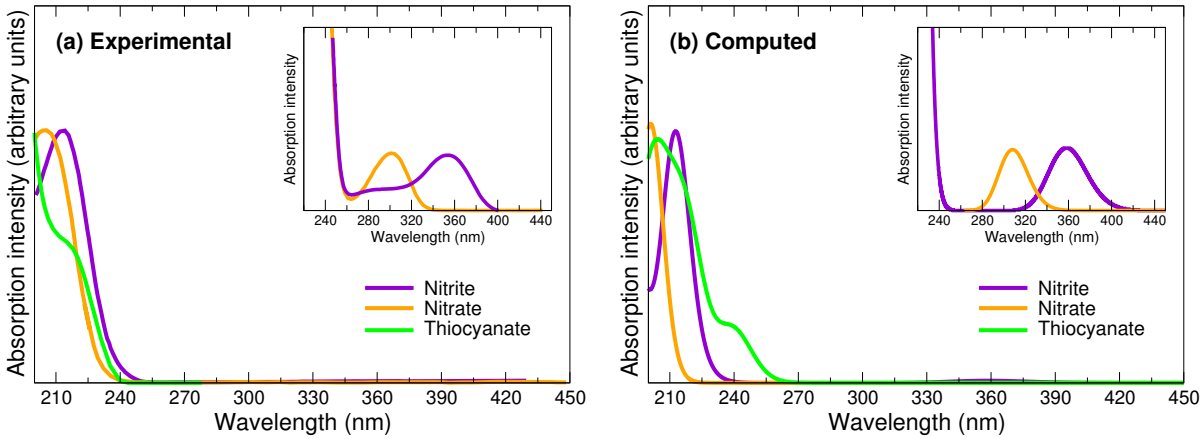

Figure 2: Experimental (left) and calculated (right) UV–Vis absorption spectra for NO_2^-, NO_3^- and SCN^- solvated ions. Experimental spectra are available in Refs. 61,62 for nitrite and nitrate, and for thiocyanate, respectively. Computed spectra were convoluted using Gaussian functions with an FWHM of 3226.17 cm^{-1}. 5 excited states were converged for nitrate, and 12 for nitrite and thiocyanate.

The absorption maxima for the three ions in aqueous solutions are summarized in Table 3. There is an outstanding agreement between experimental and computed data with slight shifts for nitrite and nitrate. The experimental thiocyanate UV–Vis spectrum shows a broad shoulder centered near 220 nm.[62,63] A closer inspection by Saykally and coworkers[63] determined one resonant wavelength at 205 nm and another weakly–resonant at 230 nm, wavelengths that are outstandingly reproduced by our calculations. The excellent match between experimental and calculated wavelengths led us to select an incident $\omega_0 = 210$ nm for the calculation of RR spectra, we also tested wavelengths in the close vicinity of 210 nm.

Before we move to the RR spectra, we take advantage of the information given by the UV–Vis spectrum regarding the excited states involved in the electronic transitions and the way the sticks are grouped together to give rise to the bands. This distinction is important because as pointed out by Asher[26] in the case of single molecules as nitrite with two absorp-

Table 3: Summary of experimental and computed absorption bands of aqueous NO_2^-, NO_3^- and SCN^-. Five explicit water molecules were used in the calculations at the B3LYP/6–311++G(d,p) level.

Ion	**Wavelength (nm)**			**Comments**
	Experimental	**Ref.**	**Computed**	
NO_2^-	212.8	61	212.7	intense band
	353.9		355.4	weak band
NO_3^-	205.6	61	201.3	intense band
	301.6		307.3	weak band
SCN^-	≈ 220	62,63	204.3	—
			239.8	—

tion bands deriving from the same chromophoric segment, changes in the RR spectra will arise from differences in the structure of the excited states associated with the two electronic transitions because the different excited states have a different coupling with the ground state vibrational motion. Figure 3 shows the sticks associated with the different transitions and their oscillator strengths, colored according to every specific excited state. It can be observed that the weak band at 353.9 nm is the result of a transition from from S_0, the ground state, to S_1, the first excited state (black sticks) which has been attributed to the $n_N \rightarrow \pi^*$ transition.[32] Zuo and Deng[64] reported a weak shoulder around 292 which correspond to the cyan sticks in the computed spectrum. The main band centered at 212.8 nm is way more complex because it is due to a superposition of sticks associated to transitions from S_0 to S_3, $S_4, \cdots$, up to S_7. These sticks have been attributed to the $\pi_2 \rightarrow \pi^*$, $n_{O_2} \rightarrow \pi^*$, and $n_{O_1} \rightarrow \pi^*$ transitions in our previous work.[32] Therefore, if the incident wavelength for the computation of RR spectra for microsolvated nitrite is chosen in the range of 250 nm $< \omega_0 <$ 353.9 nm, only the first two excited states should be taken into consideration, and, computations with excitations associated to the brighter transition (200 nm $< \omega_0 <$ 250 nm) must include S_3, S_4, S_5, S_6, and S_7.

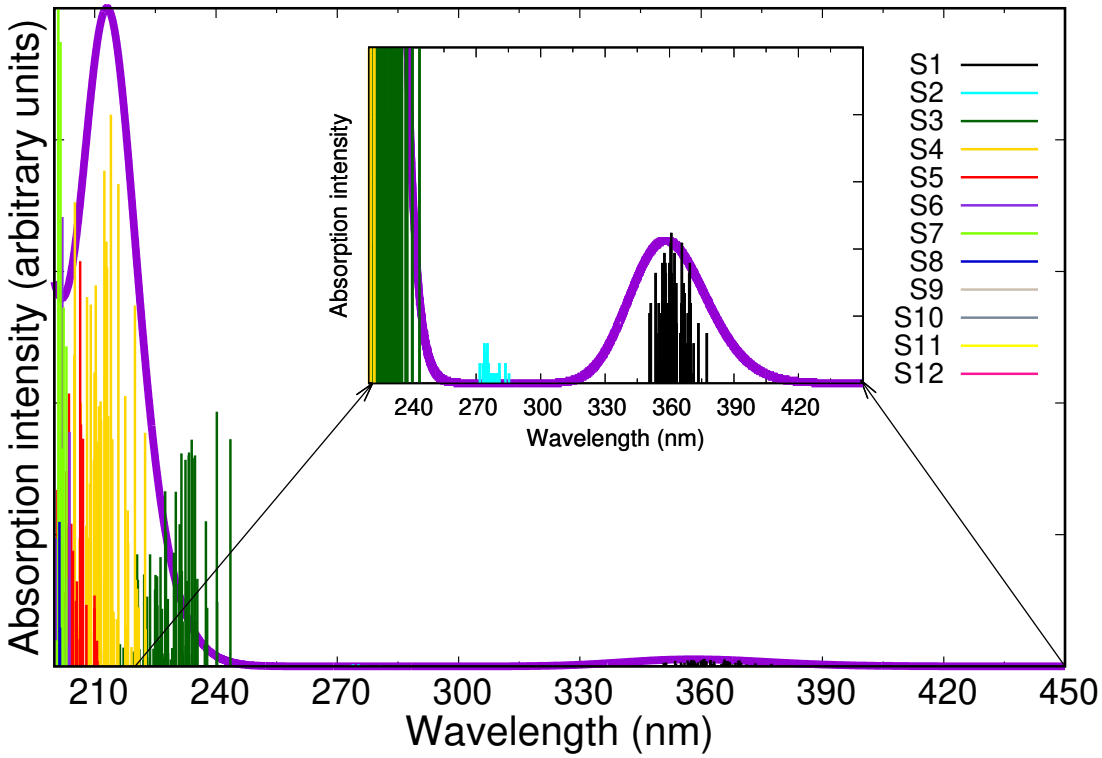

Figure 3: Computed absorption sticks and convoluted spectra for S_i, the excited states of $[NO_2\,(H_2O)_5]^-$ clusters at B3LYP/6–311++G(d,p)/PCM.

The same procedure to assign excited states to a particular band or range runs for the nitrate and thiocyanate clusters (see Figures S8, S9), for which the molecular orbitals (MOs) involved in the transitions are displayed in Figure 4 in the main text and in Figure S10 in the ESI. One noteworthy detail, not exclusive of the nitrite case, is that the molecular orbitals of the solvent heavily contribute to the main absorption bands, hence proper account of explicit water molecules is mandatory to reproduce the experimental spectra. This observation, recently exposed by the present authors,[32] prevents the application of common and/or polarizable QM/MM approaches to calculate spectra of aqueous solutions of NO_2^-, and by extension, of any microsolvated ion in which the MOs of the solvent contribute to the absorption bands.

Molecular Orbital	ASCEC + PCM	λ (nm)	Electronic transitions
LUMO (π*)	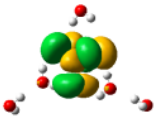	301.6	
HOMO (n)	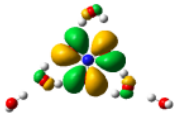		
HOMO - 1 (π_2)	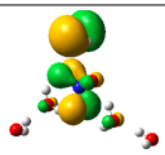	205.6	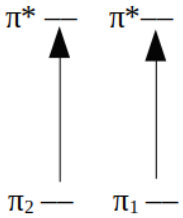
HOMO - 5 (π_1)	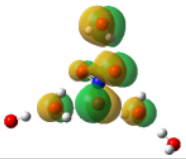		
HOMO - 8	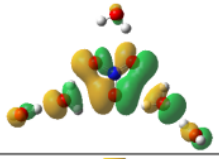		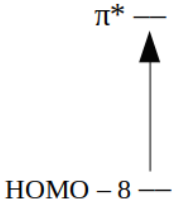
HOMO - 9	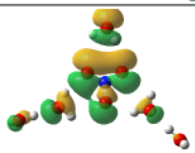		
HOMO - 11	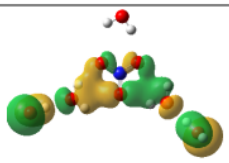		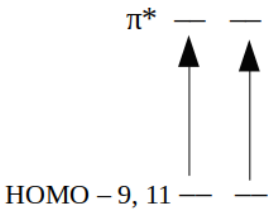

Figure 4: Molecular orbitals involved in UV–Vis transitions in the putative global minimum of the $[NO_3(H_2O)_5]^-$ potential energy surface. Isovalue=0.02

3.3 RR spectroscopy

Experimental[28] and computed[65,66] RR spectra are available for nitrate aqueous solutions. Only the experimental RR spectrum has been reported for nitrite,[28] thus, these two ions are ideal candidates to test our protocol before proceeding to its application to more challenging cases, such a s SCN^-, for which no RR spectrum of any kind has been reported. We proceeded accordingly, and as described above, we used $\omega_0 = 210$ nm. In addition, for the sake of completeness, we also calculated the far from resonance $\omega_o = 532$ nm conventional Raman spectra for all $[Anion(H_2O)_5]^-$ clusters, the corresponding convoluted profiles are shown in Figures S12 and S13. Although the agreement is not quantitative at this wavelength, the calculated Raman spectra do capture most of the characteristic signals of the experimental spectra. Nevertheless, we clearly see the enhancement of signals in the RR spectra at $\omega_0 =$ 210 nm for the three anions as shown in Figures S16, S17, and S18 in the ESI. For nitrate, the most extreme case, this enhancement goes up to 3 orders of magnitude for the symmetric vibrations. We analyze the RR spectra for each anion on an individual basis next and culminate with the superposition of the three spectra, which we relate to aqueous samples containing the three pollutants.

3.3.1 Nitrite

Belonging to the C_{2v} point group, the bare nitrite ion has the three normal modes displayed in Figure 5. The two stretchings (symmetric, ν_1, and antisymmetric, ν_2) and the bending vibration (ν_3) are active in both infrared and Raman[67] and are located roughly at 1335 cm^{-1}, 1300 cm^{-1}, and 800 cm^{-1}, respectively. The RR spectra of nitrite, modeled at $\omega_0 = 210$ nm, obtained under PCM only, and for $[NO_2\,(H_2O)_5]^-$ clusters, are compared in Figure 6 against the experimental information taken from Ianoul et al.[28]. As expected, each vibrational mode produces a signal in the experimental RR spectra, there, ν_1, appearing at 1325 cm^{-1}, is the most intense one due to the fact that in Raman the dominant bands often involve totally

symmetric vibrations.[68] Indeed, this band is used in experimental methodologies for the detection and quantification of nitrite in water.[28]

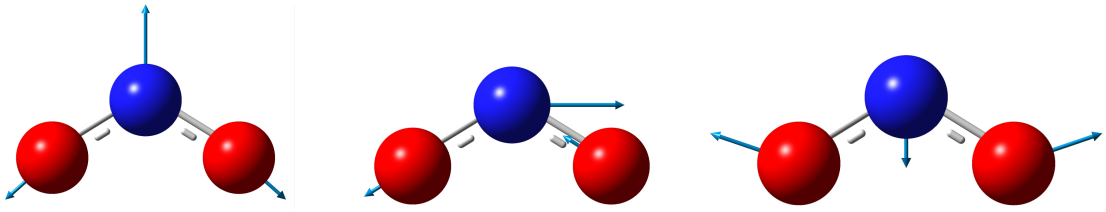

Symmetric stretching
$\nu_1 = 1334.2$ cm^{-1}

Antisymmetric stretching
$\nu_2 = 1296.8$ cm^{-1}

Bending
$\nu_3 = 799.6$ cm^{-1}

Figure 5: The normal modes for the isolated nitrite ion and their vibrational frequencies. Level of theory B3LYP/6–311++G(d,p)/PCM. Since these normal modes change when water molecules surround the ion, a depiction of them in the case of the global minimum of $[NO_2(H_2O)_5]^-$ is included in the ESI (Figure S11).

The measured RR spectrum is deceptively simple with the following assignments from the experimental group who reported it:[28] the intense band centered at ≈ 1325 nm to ν_1, the two broad bands, one centered at ≈ 1670 nm, and the other running the $\approx 630 - 900$ nm interval, to solvent vibrations. Thus, the experimental analysis includes no assignation to ν_2, ν_3 and no discussion of the shoulder adjacent to ν_1. The first obvious failure of the continuum model is that, as expected, the calculated spectrum does not recover solvent vibrations ($\omega = 1670$ nm), however, the continuum model hints at ν_3 appearing on the low energy region assigned to water vibrations while saying nothing about ν_2. We report two spectra calculated with the explicit waters in Figure 6, the green spectrum corresponds to the global minimum in the $[NO_2(H_2O)_5]^-$ PES while the red spectrum accounts for the statistical contributions from all isomers. These two spectra show peaks for all vibrations and explain the structure of the experimental spectrum as follows:

1. ν_1 is recovered at the same position and relative intensity for both spectra, however, when all isomers are considered, this band splits into two because microsolvation breaks the symmetry of the vibration leading to a smaller band to the right of the original ν_1. This observation highlights the importance of considering all structures within a given PES.

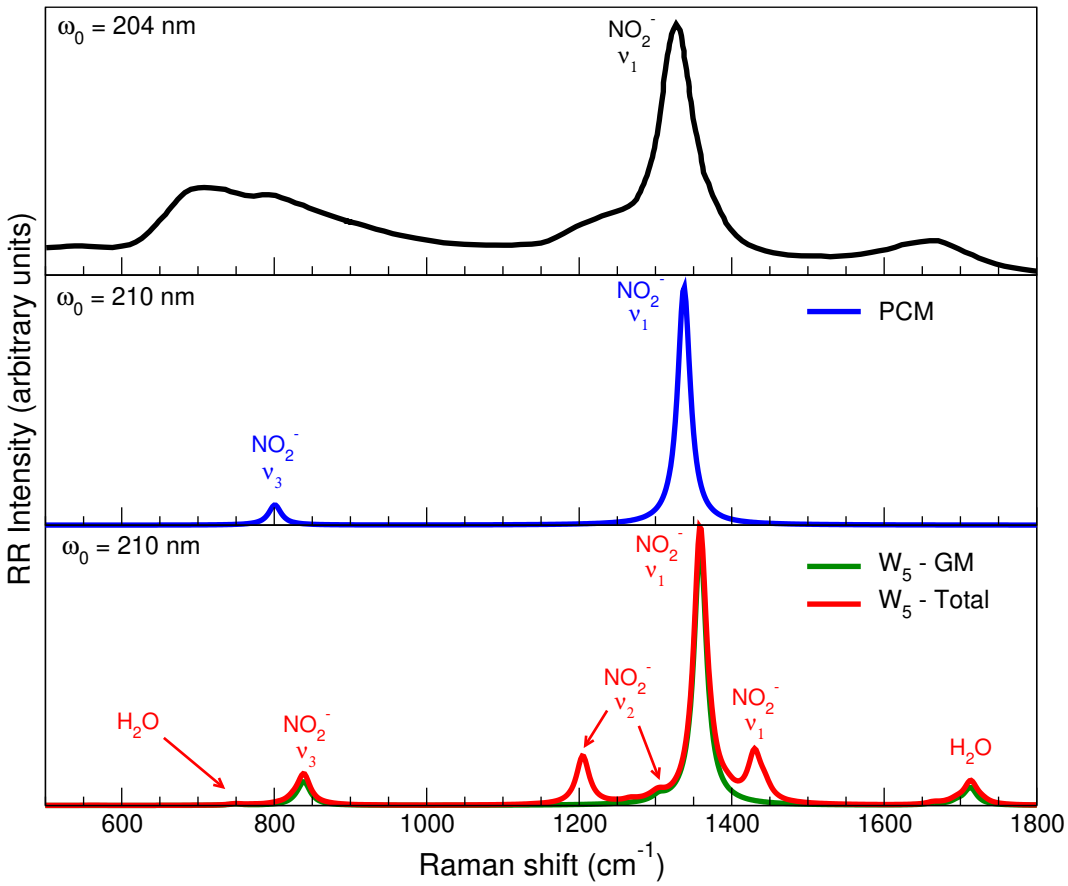

Figure 6: Experimental (top panel), computed in PCM (middle panel) and computed with explicit waters (bottom panel) RR spectra of nitrite. Calculations at B3LYP/6–311++G(d,p) level of theory and under the VG|FC approach, with $\omega_0 = 210$ nm. A 200 cm^{-1} damping factor was used for the RR intensities and Lorentzian functions with FWHM=20 cm^{-1} were employed in the convolution of the spectra. The excited states 3, 4, 5, 6 and 7 were used, because they are involved in the most intense absorption band. The experimental data was taken from Ianoul et al.[28] GM stands for the global minimum, shown in Figure 1.

2. ν_2 manifests in the shoulder to the left of ν_1. The same symmetry breaking due to microsolvation and contributions from many structures prevent the splitting into to well defined bands.

3. In agreement with the continuum solvent spectrum, ν_3 contributes to the broad band at the left of the spectrum.

4. Solvent vibrations are responsible for the broad bands to the right and left of the spectra, with the left band overlapping ν_3.

The RR spectra for nitrite microsolvated with 1 to 6 molecules of water can be found in the ESI (Figure S14), and as foreseen from the UV–Vis spectra, in the $x = 5, 6$ cases, the simulated spectra are almost identical. Furthermore, except for slight differences in a couple of intensities (Figure S15), the RR spectrum calculated at 210 nm remains almost unaltered when it is calculated with the smaller set of five excited states mentioned above or with 12 excited states. This observation is corroborated by the fact that the remaining excited states are far removed from the absorption band located at 210 nm (Figure 3).

3.3.2 Nitrate

The Raman spectrum for nitrate in aqueous solution is particularly well documented,[20–24,69] and the Resonance Raman has also been reported because of its importance in the analysis of aqueous samples.[28,65,66] The highly symmetric nitrate ion belongs to the D_{3h} point group. Its six normal modes are shown in Figure 7, including two pairs (ν_3, ν_4) and (ν_5, ν_6) of degenerate vibrations. It is known from early works[67,70] that ν_1, the N–O symmetric stretching, and ν_2, the out–of–plane deformation, are both Raman active and become infrared active in aqueous solution as well. In addition, ν_3, ν_4, ν_5, and ν_6 are active in IR, Raman, and RR. The experimental and computed spectra for the solvated ion are collected in Figure 8.

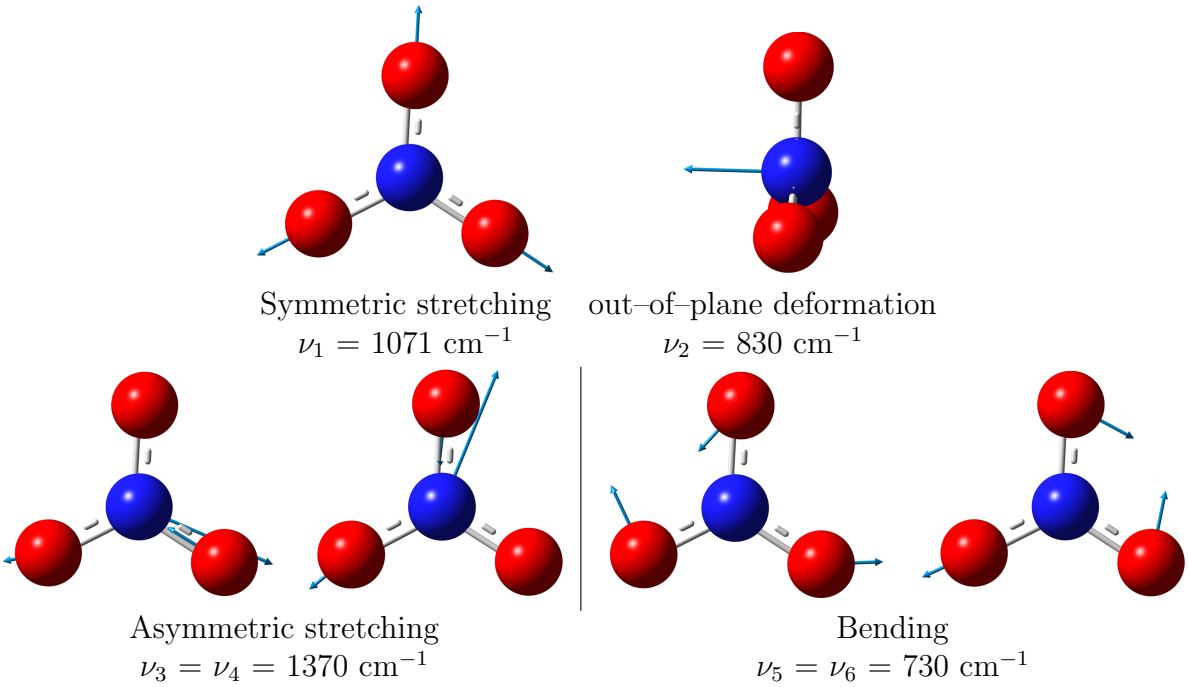

Figure 7: The normal modes for nitrate ion and their vibrational frequencies. Level of theory B3LYP/6–311++G(d,p)/PCM.

The three experimental spectra[28,65,66] are fully consistent with each other and offer the following band assignments: ν_1 is the most intense band centered at ≈ 1044 cm^{-1}. No experimental spectrum of aqueous nitrate assigns ν_2. Just as in the RR spectrum of NO_2^-, the band to the far right is due to the solvent as is the broad band to the far left, however, the latter contains contributions from ν_5, ν_6 near 723 cm^{-1}, according to Waterland and Kelley[65]. The broad band around 1400 cm^{-1} is the result of ν_3 and ν_4 splitting because of symmetry breaking due to solvation. Breaking of the symmetry of the ν_3, ν_4 vibrations is even observed in the solid state, with the size of the splitting being directly dependent on the identity of the cation in the salt.[66]

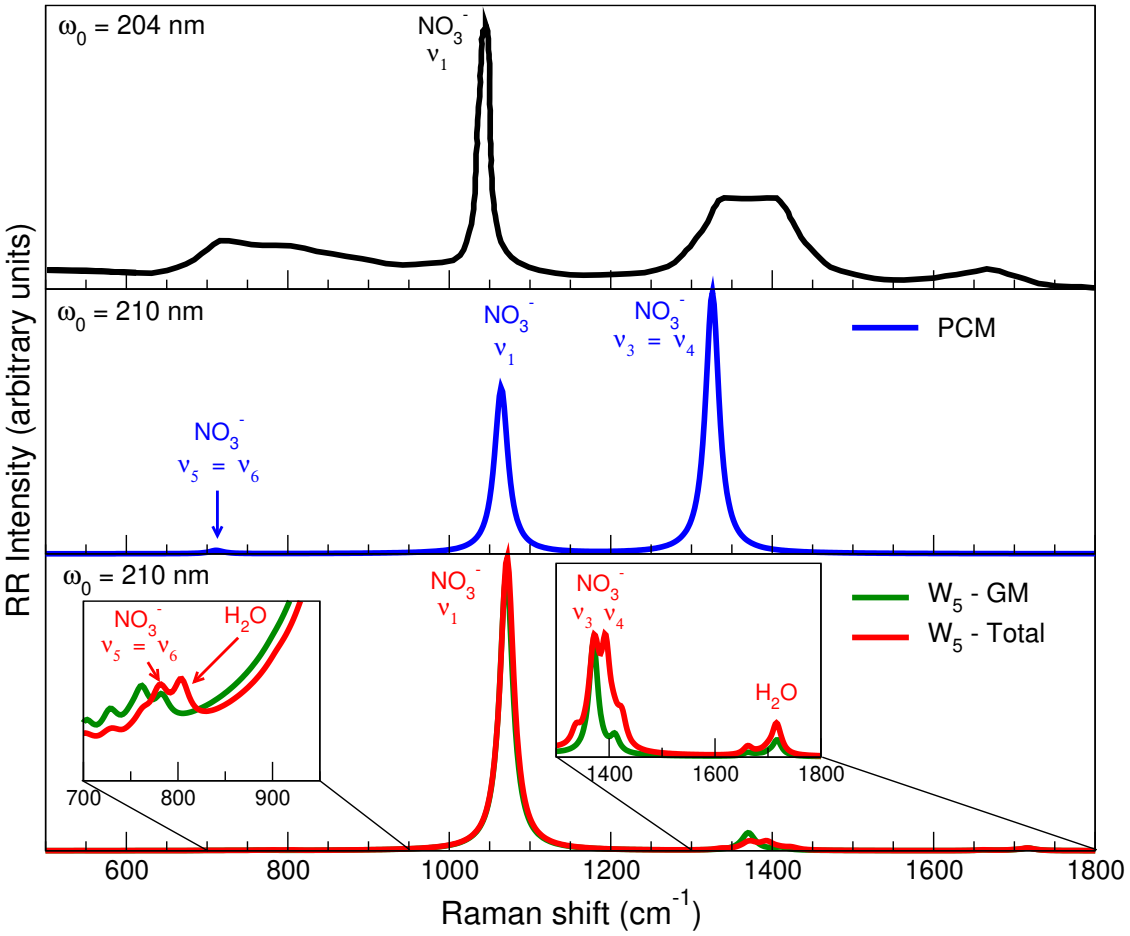

Figure 8: Experimental (top panel), computed in PCM (middle panel) and computed with explicit waters (bottom panel) RR spectra of nitrate. Calculations at B3LYP/6–311++G(d,p) level of theory and under the VG|FC approach, with $\omega_0 = 210$ nm. A 200 cm^{-1} damping factor was used for the RR intensities and Lorentzian functions with FWHM=20 cm^{-1} were employed in the convolution of the spectra. The excited states 2, 3, 4 and 5 were used, because they are involved in the most intense absorption band. The experimental data was taken from Ianoul et al.[28]. GM stands for the global minimum, shown in Figure 1.

The calculated PCM spectrum picks all nitrate vibrations except ν_2, but gives wrong intensities because the lack of explicit waters prevents the symmetry breaking leading to the split of ν_3, ν_4 and of ν_5, ν_6 and prevents the involvement of water orbitals in the transitions (see Figure 4). The spectra of microsolvated of NO_3^- do not pick ν_2 and exhibit the following features:

1. ν_1 is the most intense band. It is remarkable that microsolvation explains why in the experimental spectrum this band does not exhibit solvent induced splitting due to

symmetry breaking: as seen in Figure 1, the chemical environment of the three N–O is equivalent even after solvation.

2. A splitting of the degenerate ν_3, ν_4 modes is only observed in the spectrum calculated with contributions from all isomers, not just the global minimum

3. Water vibrations are heavily shifted

4. The broad band to the left includes water vibrations and splitting of ν_5, ν_6

In fact, closer inspection of the RR spectrum with explicit waters (bottom panel in Figure 8 and better seen from the Boltzmann weighted spectrum) highlights such a splitting and some water vibrations in that spectral region. In this regard, there are *ab initio* calculations on nitrate clusters supporting and explaining the splittings.[65,66]

3.3.3 Thiocyanate

As shown above, only when considering explicit waters, it is possible to reproduce the main and specific characteristics of the experimental spectra for nitrite and nitrate. Thanks to the remarkable agreements between experiment and computations, we now move to the prediction of the RR spectrum for aqueous thiocyanate, which, to the best of our knowledge, has not been reported from neither the theoretical or experimental points of view. For this ion we first consider the four vibrational modes pictured in Figure 9.

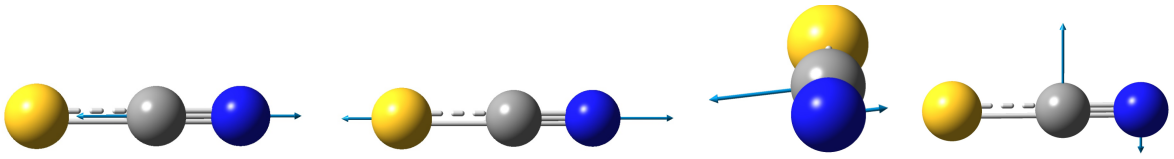

C–N Stretching
$\nu_1 = 2132$ cm^{-1}

S–C Stretching
$\nu_2 = 730$ cm^{-1}

Bending
$\nu_3 = \nu_4 = 459$ cm^{-1}

Figure 9: The normal modes for the thiocyanate ion and their vibrational frequencies. Level of theory B3LYP/6–311++G(d,p)/PCM.

Instead of isolated S–C and C≡N bonds, the electronic structure of $[SCN]^-$ comprises π orbitals delocalizing the excess charge over the three centers, thus, a more appropriate

description is $[S{\equiv}C{\equiv}N]^-$. Because of its strength, the stretching of $C{\equiv}N$, ν_1, is expected to have the highest vibrational frequency, which is reported at around 2040 cm^{-1}.[71] It has been previously determined[67] that the position of this band can vary up to 17 cm^{-1} in KSCN samples, depending on whether the measurement is carried out in ATR or in Raman, in solid state or in aqueous solution. Similarly, the band for the $C{\equiv}S$ stretching, ν_2, around 740 cm^{-1}, can shift between 690 and 720 cm^{-1} depending on the type of metal attached to the sulfur atom.[72] There are also two degenerate bending vibrations: out–of–plane ν_3, and in–plane ν_4, at ≈ 450 cm^{-1}. The computed spectra for $[SCN]^-$ embedded in a continuum solvent and with five explicit waters are displayed in Figure 10. The corresponding assignments of the normal modes are also included.

From Figure 10, we can highlight two interesting points: first, there are large differences between the obtained spectra with both solvation models, quite appreciable in the relative intensities between the peaks. The PCM spectrum only shows two bands arising from $C{\equiv}N$ (ν_1) and $S{\equiv}C$ (ν_2) stretchings. The degenerate ν_3, ν_4 bands are picked by the PCM computations but with negligible intensities in the spectrum, however, remarkably, these bands, with a tiny splitting not apparent with the FWHM used, are well defined when explicit waters are taken into account, as visualized in the bottom panel of Figure 10. As previously discussed, PCM cannot capture the bands associated with water vibrations, nonetheless, those vibrations are identified at around 1700 cm^{-1} and in the $\approx 600 - 1000$ cm^{-1} interval in the cluster spectra. Second, we clearly see a splitting of the ν_1 and ν_2 peaks in the spectra with explicit waters. The mandatory inclusion of all meaningful structures in the convoluted spectrum is beautifully exemplified in the case of $[SCN\,(H_2O)_5]^-$. Indeed, the separate spectra for W_5S_1 with population of 36.8% and W_5S_2 with a 23.3% population (Figure 1), exhibit a small but appreciable shift for all bands, which show up as pairs of split peaks in the convoluted spectrum. In this scenario, the exhaustive configurational sampling helps us to understand that the division of the peaks is not only due to the microsolvation induced loss of symmetry of the vibrations, as happens in the nitrate case, but also to the

existence of several structures contributing to the total spectrum.

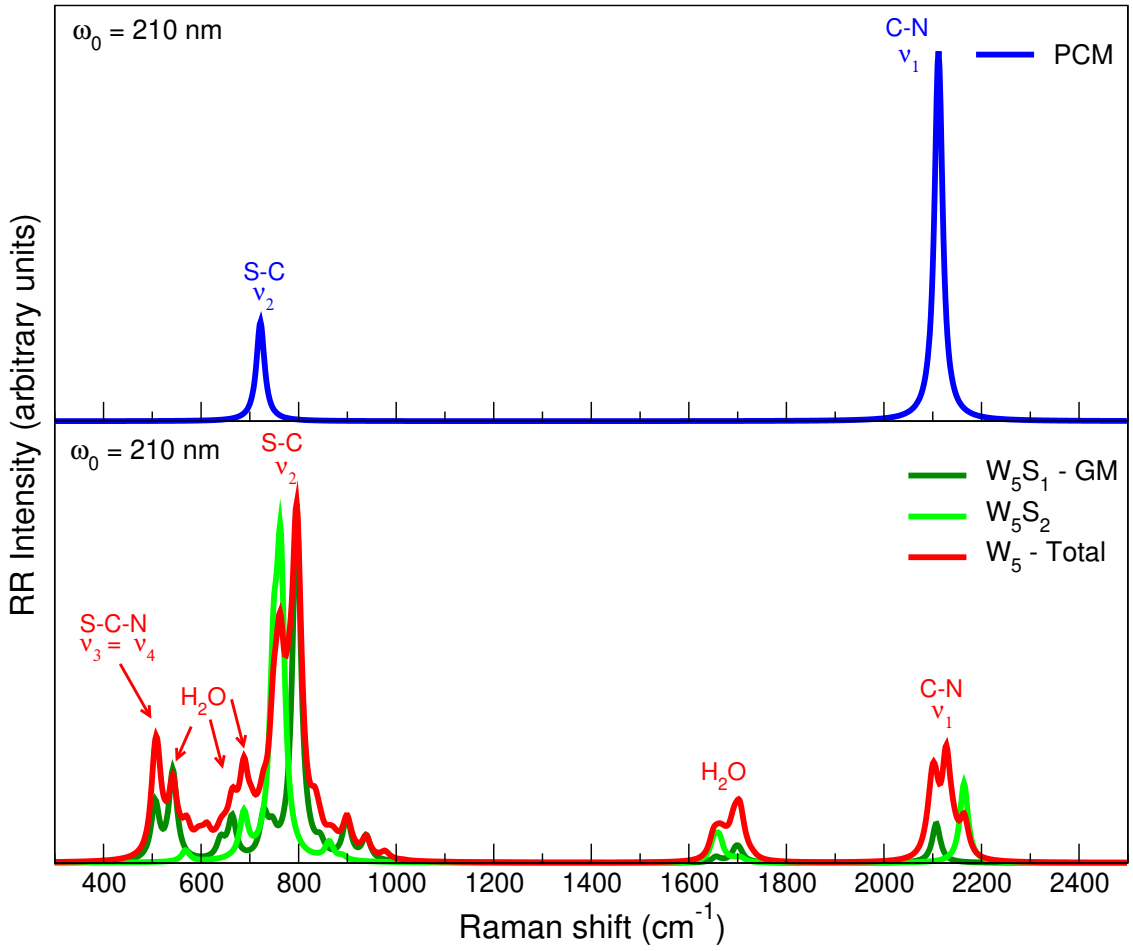

Figure 10: RR spectra of thiocyanate computed in PCM (top panel) and with explicit waters (bottom panel). Calculations at B3LYP/6–311++G(d,p) level of theory and under the VG|FC approach, with $\omega_0 = 210$ nm. A 200 cm^{-1} damping factor was used for the RR intensities and Lorentzian functions with FWHM=20 cm^{-1} were employed in the convolution of the spectra. The first 12 excited states were used. GM_1 and GM_2 stand for the global minima, shown in Figure 1.

Although we did not find RR measurements for thiocyanate, we find it useful to compare our computed spectra against the Raman spectrum of $[SCN]^-$ in an aqueous solution containing 5% of methanol reported by Wahab and Mahiuddin [73]. Figure S13 shows the calculated Raman spectrum obtained with the 63 $[SCN\,(H_2O)_5]^-$ clusters. A very good match to the experimental data is clearly seen in the reproduction of the signal at 2050 cm^{-1}.

3.3.4 RR of the three ions combined

It has been found that the RR effect can lead to significant selectivity in Raman spectral measurements.[26,74] In order to find specific wavelengths to be used in RR that will allow the simultaneous identification of NO_2^-, NO_3^- and $[SCN]^-$ ions in water samples, we used the information provided by the UV–Vis spectra in Figure 2 and the RREPs presented in Figure 11. Raman intensities reflect the properties of a particular electronic state because its vibrational levels dominate the scattering process when the incident light is properly tuned,[68] therefore, we investigate in Figure 11(a) the influence of different incident wavelengths on the intensities of the normal mode ν_1 for the global minimum of $[NO_2\,(H_2O)_5]^-$. A comparison of the bars indicates that both absolute and relative RR intensities vary with the incident wavelength.[75] The biggest peaks of RR intensities for ν_1 take place with vibrational excitations in resonance with the electronic state, meaning 212.8 and 353.9 nm for the nitrite case. In particular, the intensity of ν_1 is 10^5 times higher approaching the main absorption band when compared to the intensity of the 353.9 band.

Waterland and Kelley[65] presented experimental and empirical modeling of the RREP of NO_3^- in several solvents from 204 to 246 nm. Later, the same authors calculated the RREPs using *ab initio* methods on the same interval of wavelengths for the normal modes of $[NO_3\,(H_2O)_2]^-$. Essentially, for normal modes ν_1 and ν_3, ν_4, the highest RR intensity was observed to occur around 205 nm (absorption maximum in UV–Vis). In line with those results, our own RREPs for ν_1 in the global minimum of $[NO_3\,(H_2O)_5]^-$, shown in Figure 11(b), reveal that resonance excitations within the nitrate absorption band produce an exceptional Raman intensity increase.

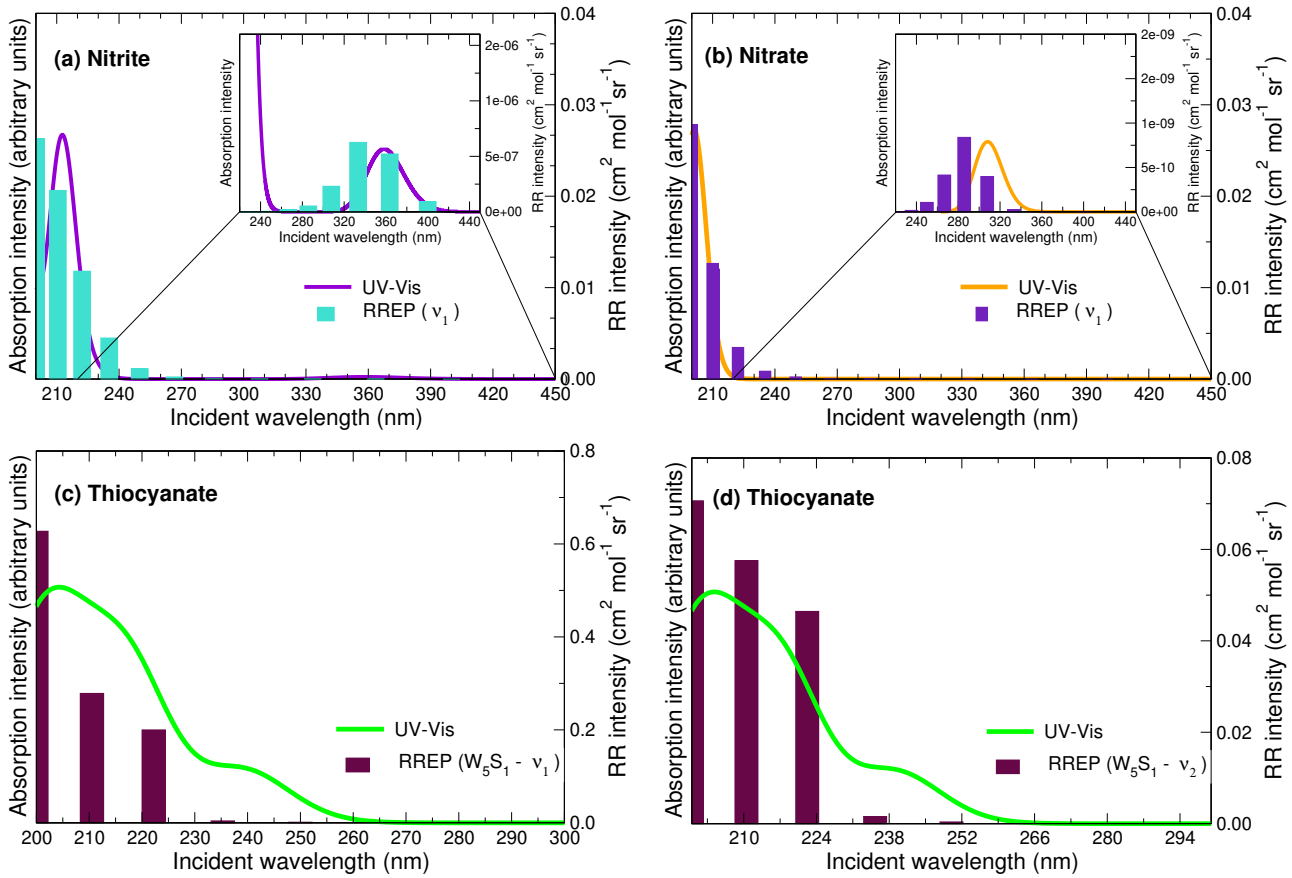

Figure 11: Calculated Resonance Raman Excitation Profile (RREP) for the vibrational mode ν_1 of the global minima of **(a)** $[NO_2\,(H_2O)_5]^-$, **(b)** $[NO_3\,(H_2O)_5]^-$ **(c)** and **(d)**$[SCN\,(H_2O)_5]^-$. For the RREP in excitation wavelengths covering the main band, the excited states 3, 4, 5, 6 and 7 were used for nitrite (2, 3, 4 and 5 for nitrite), whereas just the first excited state was taken for the RREPs in the inset. In **(c)** and **(d)**, the first 12 excited states were considered. B3LYP/6–311++G(d,p) and VG|FC were used in all cases.

In the case of thiocyanate, and given the conflicting predictions offered by the two solvation models concerning the most intense peak, we built the excitation profiles for both ν_1 and ν_2. The associated plots are shown in Figures 11(c) and (d) for W_5S_1, the putative global minimum for the microsolvation of $[SCN]^-$ with five water molecules. The corresponding plots for W_5S_2 are available in the ESI. Our results indicate that regardless of the structure (W_5S_1 vs W_5S_2), for those particular normal modes, the most critical changes in the RR intensities are primarily appreciated near 205 nm, which is the average wavelength where the intense absorption band of the ion is found.

Usually, in the absorption spectra of samples containing diverse targets, each absorption band derives from a particular analyte, and then, the vibrational Raman spectrum of the mixture could be selectively enhanced with proper changes in the excitation wavelength.[26] Here, the situation is more complicated because of the overlap between the absorption spectra in specific regions (see Figure 2), thus, it is desirable to selectively enhance just those individual signals that should end up well separated in the collective RR spectrum. After probing several incident wavelengths, our results indicate that for the particular case of complex aqueous mixtures containing nitrite, nitrate and thiocyanate, $\omega_0 = 210$ nm offers good separation and enhanced intensity of all peaks, thus, we postulate RR as a viable technique for the simultaneous detection of those three ions. To illustrate how our protocol has the potential to be applied to realistic samples containing multiple pollutants, we plotted in Figure 12 the collective RR spectra for the three ions calculated at $\omega_0 = 210$ nm. This computational protocol will remove two heavy barriers in the analysis of complex water samples: by carefully selecting the incident wavelength for RR, the protocol may be used in cases where the absorption spectra overlap, and, by the very nature of RR, the limits of detection may be pushed a few orders of magnitude. We are currently in the process of collecting experimental data for solutions containing pairs of the salts, all the salts together, different types of water (high purity water, sink water and contaminated water, e.g, water from lakes, rivers or fountains), those results will be the subject of future publications.

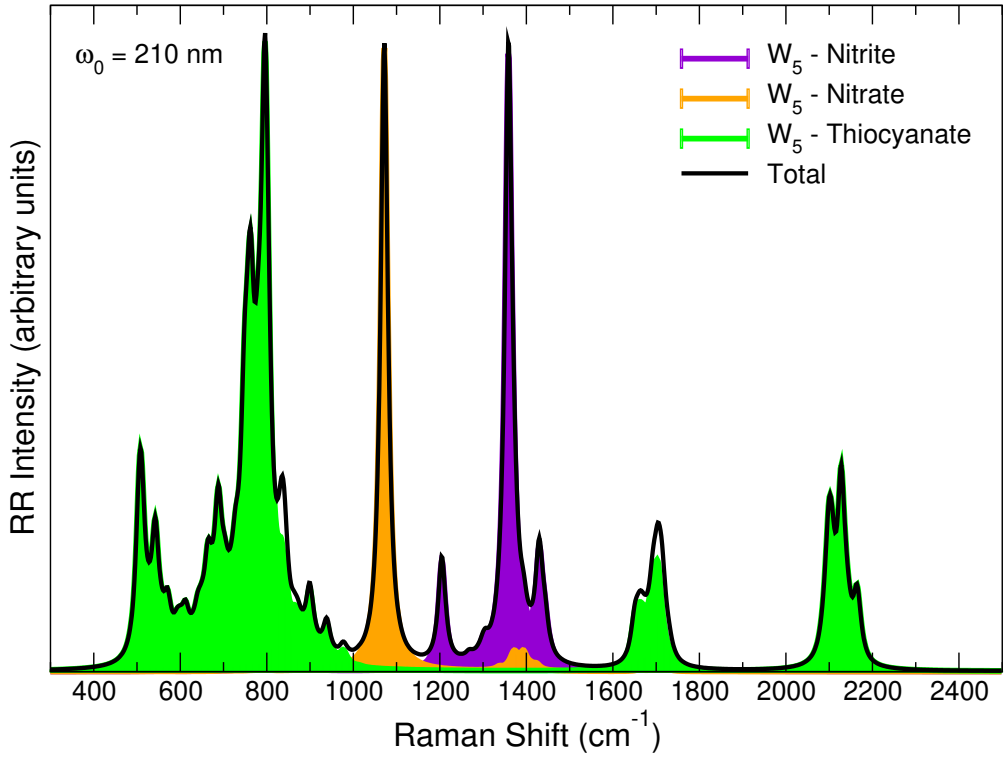

Figure 12: Computed spectra of microsolvated nitrite, nitrate and thiocyanate with five water molecules. Level of theory: B3LYP/6–311++G(d,p). The non-normalized version of these spectra can be found in Figure S19 in the ESI.

4 Summary and conclusions

In this work, we have presented a computational methodology, based on the RR technique, with the potential to guide the simultaneous identification and quantification of NO_2^-, NO_3^- and SCN^- in dilute aqueous samples, by accurately predicting their respective spectroscopic responses. The principal steps of the proposed protocol can be summarized as follows:

1. Exhaustive configurational sampling of the solvated ions
2. Optimization, classification, and vibrational characterization of the molecular clusters or snapshots
3. Calculation of UV–Vis spectra and comparison with experimental information (when available), assessing the quality of model chemistries and the different representations of the solvent
4. Selection of the excited states associated with principal electronic transitions, and selection of potential excitation wavelengths
5. Calculation of RR spectra with the excited states found in the previous step
6. Choosing of the most important normal modes with which the ions will be identified and building of the RREP to retrieve excitation wavelengths where the greatest intensities can be experimentally obtained
7. Analysis of the information given by the grouped RREPs to find the appropriate incident wavelength (ω_0) with which a sample containing the combined ions can be optimally irradiated

By employing the above set of steps we were able to reproduce the main characteristics of the RR spectra for nitrite and nitrate and predicted the RR spectrum for aqueous

thiocyanate. We demonstrate that by setting the incident radiation to 210 nm it is possible to simultaneously detect all three ions. A rigorous configurational sampling of the solute$\cdots$solvent microclusters, and proper accounts of solvent are of paramount importance in the simulation of Resonance Raman spectra. In particular, for nitrite, nitrate and thiocyanate, explicit water molecules improved in all cases the agreement with experimental data. Our analysis strongly suggests that the popular continuum solvation models, which are often employed without further validation, might inaccurately predict intensities.

Our computational methodology can aid in the design of protocols and experimental setups for the evaluation of water quality as it relates to the presence of NO_2^-, NO_3^- and SCN^-. We further hope to extend the designed protocol to other ions of interest in the control of a much wider array of emerging contaminants with the explicit benefits of simultaneously detecting pollutants whose absorption spectra overlap and pushing detection limits to lower concentrations. When tackling more general cases, further research may be needed in order to describe some of the variables involved in the experiments, such as the changes in intensities with varying concentrations since we are microsolvating just one ion in every case. Likewise, structural and spectroscopic effects of the ions on each other were not considered for the mixture, and a Molecular Dynamics simulation of the combined ions would be the first step in that regard. These aspects will be addressed in future work.

Acknowledgement

Partial funding for this project from H2020-MSCA-ITN-2017 European Training Network "Computational Spectroscopy In Natural sciences and Engineering" (COSINE), grant number 765739 is acknowledged. Internal support from Universidad de Antioquia via "Estrategia para la sostenibilidad" is also acknowledged. LU thanks Universidad de Antioquia for her graduate scholarship.

Supporting Information Available

Description of ASCEC runs. Structural motifs. Cartesian coordinates for the equilibrium structures of thiocyanate clusters afforded by ASCEC. Binding energies of diverse systems. UV–Vis, Raman and RREP spectra for $[NO_3\,(H_2O)_5]^-$ and $[SCN\,(H_2O)_5]^-$. UV–Vis spectra for the isolated ions in PCM. RR spectra for $[NO_2\,(H_2O)_x]^-$ with x from 1 to 6. RR spectra for $[NO_2\,(H_2O)_5]^-$ with 5 and 12 excited states. Comparison of Raman and RR intensities for the three ions. RREPs for the two global minima in the $[SCN\,(H_2O)_5]^-$ case. Non-normalized total spectra of the three ions combined.

References

(1) Thomas, N. C. The early history of spectroscopy. *Journal of chemical education* **1991**, *68*, 631.

(2) He, Y.; Tang, L.; Wu, X.; Hou, X.; Lee, Y.-I. Spectroscopy: the best way toward green analytical chemistry? *Applied Spectroscopy Reviews* **2007**, *42*, 119–138.

(3) Fortenberry, R. C. Quantum astrochemical spectroscopy. *International Journal of Quantum Chemistry* **2017**, *117*, 81–91.

(4) Li, Z.; Wang, J.; Li, D. Applications of Raman spectroscopy in detection of water quality. *Applied Spectroscopy Reviews* **2016**, *51*, 333–357.

(5) Kumar, M.; Borah, P.; Devi, P. *Inorganic Pollutants in Water*; Elsevier, 2020; pp 33–49.

(6) Erisman, J. W.; Sutton, M. A.; Galloway, J.; Klimont, Z.; Winiwarter, W. How a century of ammonia synthesis changed the world. *Nature Geoscience* **2008**, *1*, 636–639.

(7) Canfield, D. E.; Glazer, A. N.; Falkowski, P. G. The evolution and future of Earth's nitrogen cycle. *science* **2010**, *330*, 192–196.

(8) Harper, D. M. *Eutrophication of freshwaters*; Springer, 1992.

(9) Mohseni-Bandpi, A.; Elliott, D. J.; Zazouli, M. A. Biological nitrate removal processes from drinking water supply-a review. *Journal of environmental health science and engineering* **2013**, *11*, 35.

(10) Wang, J.; Song, M.; Chen, B.; Wang, L.; Zhu, R. Effects of pH and H2O2 on ammonia, nitrite, and nitrate transformations during UV254nm irradiation: Implications to nitrogen removal and analysis. *Chemosphere* **2017**, *184*, 1003–1011.

(11) Liu, G.; You, S.; Ma, M.; Huang, H.; Ren, N. Removal of nitrate by photocatalytic denitrification using nonlinear optical material. *Environmental science & technology* **2016**, *50*, 11218–11225.

(12) Shaban, Y. A.; El Maradny, A. A.; Al Farawati, R. K. Photocatalytic reduction of nitrate in seawater using C/TiO2 nanoparticles. *Journal of Photochemistry and Photobiology A: Chemistry* **2016**, *328*, 114–121.

(13) IARC, Ingested Nitrate and Nitrite and Cyanobacterial Peptide Toxins. *IARC Monographs on the Evaluation of Carcinogenic Risks to Humans* **2010**, *94*, 45–325.

(14) Mirvish, S. S. Role of N-nitroso compounds (NOC) and N-nitrosation in etiology of gastric, esophageal, nasopharyngeal and bladder cancer and contribution to cancer of known exposures to NOC. *Cancer letters* **1995**, *93*, 17–48.

(15) Brauer, V.; Below, H.; Kramer, A.; Fuhrer, D.; Paschke, R. The role of thiocyanate in the etiology of goiter in an industrial metropolitan area. *European journal of endocrinology* **2006**, *154*, 229–235.

(16) Laurberg, P.; Pedersen, I. B.; Carlé, A.; Andersen, S.; Knudsen, N.; Karmisholt, J. *Comprehensive Handbook of Iodine*; Elsevier, 2009; pp 275–283.

549 (17) Boyland, E.; Nice, E.; Williams, K. The catalysis of nitrosation by thiocyanate from
550 saliva. *Food and cosmetics toxicology* **1971**, *9*, 639–643.

551 (18) APHA, APHA Standard Method 4500—NO2-. B. 1998.

552 (19) ASTM, ASTM D4193-08(2020)e1, Standard Test Method for Thiocyanate in Water.
553 2020.

554 (20) Lombardi, D. R.; Wang, C.; Sun, B.; Fountain III, A. W.; Vickers, T. J.; Mann, C. K.;
555 Reich, F. R.; Douglas, J. G.; Crawford, B. A.; Kohlasch, F. L. Quantitative and qualita-
556 tive analysis of some inorganic compounds by Raman spectroscopy. *Applied spectroscopy*
557 **1994**, *48*, 875–883.

558 (21) Ahmadjian, M.; Brown, C. W. Feasibility of remote detection of water pollutants and oil
559 slicks by laser-excited Raman spectroscopy. *Environmental science & technology* **1973**,
560 *7*, 452–453.

561 (22) Baldwin, S. F.; Brown, C. W. Detection of ionic water pollutants by laser excited
562 Raman spectroscopy. *Water Research* **1972**, *6*, 1601–1604.

563 (23) Cunningham, K. M.; Goldberg, M. C.; Weiner, E. R. Investigation of detection limits for
564 solutes in water measured by laser Raman spectrometry. *Analytical Chemistry* **1977**,
565 *49*, 70–75.

566 (24) Furuya, N.; Matsuyuki, A.; Higuchi, S.; Tanaka, S. Determination of nitrate ion in waste
567 and treated waters by laser raman spectrometry. *Water Research* **1979**, *13*, 371–374.

568 (25) Gajaraj, S.; Fan, C.; Lin, M.; Hu, Z. Quantitative detection of nitrate in water and
569 wastewater by surface-enhanced Raman spectroscopy. *Environmental monitoring and*
570 *assessment* **2013**, *185*, 5673–5681.

571 (26) Asher, S. A. UV resonance Raman spectroscopy for analytical, physical, and biophysical
572 chemistry. Part 1. *Analytical chemistry* **1993**, *65*, 59–66.

(27) Egidi, F.; Bloino, J.; Cappelli, C.; Barone, V. A robust and effective time-independent route to the calculation of resonance raman spectra of large molecules in condensed phases with the inclusion of Duschinsky, Herzberg–Teller, anharmonic, and environmental effects. *Journal of chemical theory and computation* **2014**, *10*, 346–363.

(28) Ianoul, A.; Coleman, T.; Asher, S. A. UV resonance Raman spectroscopic detection of nitrate and nitrite in wastewater treatment processes. *Analytical Chemistry* **2002**, *74*, 1458–1461.

(29) Agency, U. S. E. P. Final Report: A Low-Cost UV Raman Instrument Measuring Nitrate and Nitrite for Improved Operation and Control of Nitrification/Denitrification Treatment Processes. `https://cfpub.epa.gov/ncer_abstracts/index.cfm/fuseaction/display.abstractDetail/abstract_id/7482/report/F`.

(30) Giovannini, T.; Egidi, F.; Cappelli, C. Molecular spectroscopy of aqueous solutions: A theoretical perspective. *Chemical Society Reviews* **2020**, *49*, 5664–5677.

(31) Giovannini, T.; Egidi, F.; Cappelli, C. Theory and algorithms for chiroptical properties and spectroscopies of aqueous systems. *Phys. Chem. Chem. Phys.* **2020**, *22*, 22864–22879.

(32) Uribe, L.; Gómez, S.; Giovannini, T.; Egidi, F.; Restrepo, A. An efficient and robust procedure to calculate absorption spectra of aqueous charged species applied to NO 2-. *Physical Chemistry Chemical Physics* **2021**,

(33) Flórez, E.; Acelas, N.; Ibargüen, C.; Mondal, S.; Cabellos, J. L.; Merino, G.; Restrepo, A. Microsolvation of NO_3^-: structural exploration and bonding analysis. *RSC Adv.* **2016**, *6*, 71913–71923.

(34) Gonzalez, J. D.; Florez, E.; Romero, J.; Reyes, A.; Restrepo, A. Microsolvation of Mg^{2+}, Ca^{2+}: strong influence of formal charges in hydrogen bond networks. *J. Mol. Model.* **2013**, *19*, 1763–1777.

(35) Egidi, F.; Giovannini, T.; Del Frate, G.; Lemler, P. M.; Vaccaro, P. H.; Cappelli, C. A combined experimental and theoretical study of optical rotatory dispersion for (R)-glycidyl methyl ether in aqueous solution. *Phys. Chem. Chem. Phys.* **2019**, *21*, 3644–3655.

(36) Giovannini, T.; Riso, R. R.; Ambrosetti, M.; Puglisi, A.; Cappelli, C. Electronic transitions for a fully polarizable qm/mm approach based on fluctuating charges and fluctuating dipoles: linear and corrected linear response regimes. *J. Chem. Phys.* **2019**, *151*, 174104.

(37) Puglisi, A.; Giovannini, T.; Antonov, L.; Cappelli, C. Interplay between conformational and solvent effects in UV-visible absorption spectra: Curcumin tautomers as a case study. *Physical Chemistry Chemical Physics* **2019**, *21*, 15504–15514.

(38) Gómez, S.; Giovannini, T.; Cappelli, C. Absorption spectra of xanthines in aqueous solution: A computational study. *Physical Chemistry Chemical Physics* **2020**, *22*, 5929–5941.

(39) Pérez, J. F.; Florez, E.; Hadad, C. Z.; Fuentealba, P.; Restrepo, A. Stochastic Search of the Quantum Conformational Space of Small Lithium and Bimetallic Lithium–Sodium Clusters. *The Journal of Physical Chemistry A* **2008**, *112*, 5749–5755.

(40) Pérez, J. F.; Hadad, C. Z.; Restrepo, A. Structural studies of the water tetramer. *Int. J. Quant. Chem.* **2008**, *108*, 1653–1659.

(41) Pérez, J.; Restrepo, A. ASCEC V02: Annealing Simulado con Energía Cuántica. 2008; Property, development, and implementation: Grupo de Química–Física Teórica, Instituto de Química, Universidad de Antioquia, Medellín, Colombia.

(42) Metropolis, N.; Rosenbluth, A. W.; Rosenbluth, M. N.; Teller, A. H.; Teller, E. Equation of State Calculations by Fast Computing Machines. *The Journal of Chemical Physics* **1953**, *21*, 1087–1092.

(43) Casida, M. E. *Recent Advances In Density Functional Methods: (Part I)*; World Scientific, 1995; pp 155–192.

(44) Hohenberg, P.; Kohn, W. Inhomogeneous electron gas. *Physical review* **1964**, *136*, B864.

(45) Kohn, W.; Sham, L. J. Self-consistent equations including exchange and correlation effects. *Physical review* **1965**, *140*, A1133.

(46) Runge, E.; Gross, E. K. Density-functional theory for time-dependent systems. *Physical Review Letters* **1984**, *52*, 997.

(47) Gómez, S.; Egidi, F.; Puglisi, A.; Giovannini, T.; Rossi, B.; Cappelli, C. Unlocking the power of resonance Raman spectroscopy: The case of amides in aqueous solution. *Journal of Molecular Liquids* **2021**, 117841.

(48) Hecht, L.; Nafie, L. A. Theory of natural Raman optical activity: Part I. Complete circular polarization formalism. *Molecular physics* **1991**, *72*, 441–469.

(49) Long, D. A. *The Raman Effect*; John Wiley & Sons, Ltd, 2002; Chapter 5, pp 85–152.

(50) Long, D. A. *The Raman Effect*; John Wiley & Sons, Ltd, 2002; Chapter 24, pp 471–495.

(51) Frisch, M. J.; Trucks, G. W.; Schlegel, H. B.; Scuseria, G. E.; Robb, M. A.; Cheeseman, J. R.; Scalmani, G.; Barone, V.; Petersson, G. A.; Nakatsuji, H. et al. Gaussian 16 Revision B.01. 2016; Gaussian Inc. Wallingford CT.

(52) Gómez, S.; Nafziger, J.; Restrepo, A.; Wasserman, A. Partition-DFT on the water dimer. *J. Chem. Phys.* **2017**, *146*, 074106.

(53) Ramírez, F.; Hadad, C.; Guerra, D.; David, J.; Restrepo, A. Structural studies of the water pentamer. *Chem. Phys. Lett.* **2011**, *507*, 229 – 233.

(54) Hincapié, G.; Acelas, N.; Castaño, M.; David, J.; Restrepo, A. Structural Studies of the Water Hexamer. *J. Phys. Chem. A* **2010**, *114*, 7809–7814.

(55) Baer, M. D.; Mundy, C. J. An ab initio approach to understanding the specific ion effect. *Faraday discussions* **2013**, *160*, 89–101.

(56) Schönfeld, P.; Montero, L.; Fabian, J. A combined experimental and quantum chemical study on the putative protonophoric activity of thiocyanate. *Biophysical journal* **2005**, *89*, 1504–1515.

(57) Wang, X.-B. Cluster model studies of anion and molecular specificities via electrospray ionization photoelectron spectroscopy. *The Journal of Physical Chemistry A* **2017**, *121*, 1389–1401.

(58) Mason, P.; Neilson, G.; Dempsey, C.; Barnes, A.; Cruickshank, J. The hydration structure of guanidinium and thiocyanate ions: implications for protein stability in aqueous solution. *Proceedings of the National Academy of Sciences* **2003**, *100*, 4557–4561.

(59) Botti, A.; Pagnotta, S. E.; Bruni, F.; Ricci, M. A. Solvation of KSCN in Water. *The Journal of Physical Chemistry B* **2009**, *113*, 10014–10021.

(60) Kunz, W.; Henle, J.; Ninham, B. W. 'Zur Lehre von der Wirkung der Salze'(about the science of the effect of salts): Franz Hofmeister's historical papers. *Current Opinion in Colloid & Interface Science* **2004**, *9*, 19–37.

(61) Thomas, O.; Brogat, M. *UV-Visible Spectrophotometry of Water and Wastewater*; Elsevier, 2017; pp 379–517.

(62) Petersen, P. B.; Saykally, R. J. On the nature of ions at the liquid water surface. *Annu. Rev. Phys. Chem.* **2006**, *57*, 333–364.

(63) Onorato, R. M.; Otten, D. E.; Saykally, R. J. Adsorption of thiocyanate ions to the dodecanol/water interface characterized by UV second harmonic generation. *Proceedings of the National Academy of Sciences* **2009**, *106*, 15176–15180.

(64) Zuo, Y.; Deng, Y. The near-UV absorption constants for nitrite ion in aqueous solution. *Chemosphere* **1998**, *36*, 181–188.

(65) Waterland, M. R.; Kelley, A. M. Far-ultraviolet resonance Raman spectroscopy of nitrate ion in solution. *The Journal of Chemical Physics* **2000**, *113*, 6760–6773.

(66) Waterland, M. R.; Stockwell, D.; Kelley, A. M. Symmetry breaking effects in NO 3-: Raman spectra of nitrate salts and ab initio resonance Raman spectra of nitrate–water complexes. *The Journal of Chemical Physics* **2001**, *114*, 6249–6258.

(67) Ahlijah, G.; Mooney, E. The attenuated total reflection spectra of polyatomic inorganic anions-II.: the nitrogen containing anions. *Spectrochimica Acta Part A: Molecular Spectroscopy* **1969**, *25*, 619–627.

(68) Myers, A. B. Resonance Raman intensity analysis of excited-state dynamics. *Accounts of chemical research* **1997**, *30*, 519–527.

(69) Fontana, M. D.; Mabrouk, K. B.; Kauffmann, T. H. Raman spectroscopic sensors for inorganic salts. *Spectrosc Prop Inorg Organomet Compd* **2013**, *44*, 40–67.

(70) Irish, D.; Davis, A. Interactions in aqueous alkali metal nitrate solutions. *Canadian Journal of Chemistry* **1968**, *46*, 943–951.

(71) Kinell, P.; Strandberg, B. Infrared and Raman spectra of some systems Containing thiocyanate groups. *Acta Chem. Scand* **1959**, *13*, 1607–1622.

(72) Clark, R.; Williams, C. S. Infra-red spectra (3000-200 cm- 1) of metal-isothiocyanate complexes. *Spectrochimica Acta* **1966**, *22*, 1081–1090.

690 (73) Wahab, A.; Mahiuddin, S. Solvation phenomena of potassium thiocyanate in methanol–
691 water mixtures. *Journal of solution chemistry* **2005**, *34*, 537–560.

692 (74) Gómez, S.; Rojas-Valencia, N.; Giovannini, T.; Restrepo, A.; Cappelli, C. Ring Vi-
693 brations to Sense Anionic Ibuprofen in Aqueous Solution as Revealed by Resonance
694 Raman. *Molecules* **2022**, *27*.

695 (75) Asher, S. A. UV resonance Raman spectroscopy for analytical, physical, and biophysical
696 chemistry. Part 2. *Analytical chemistry* **1993**, *65*, 201A–210A.

697 TOC

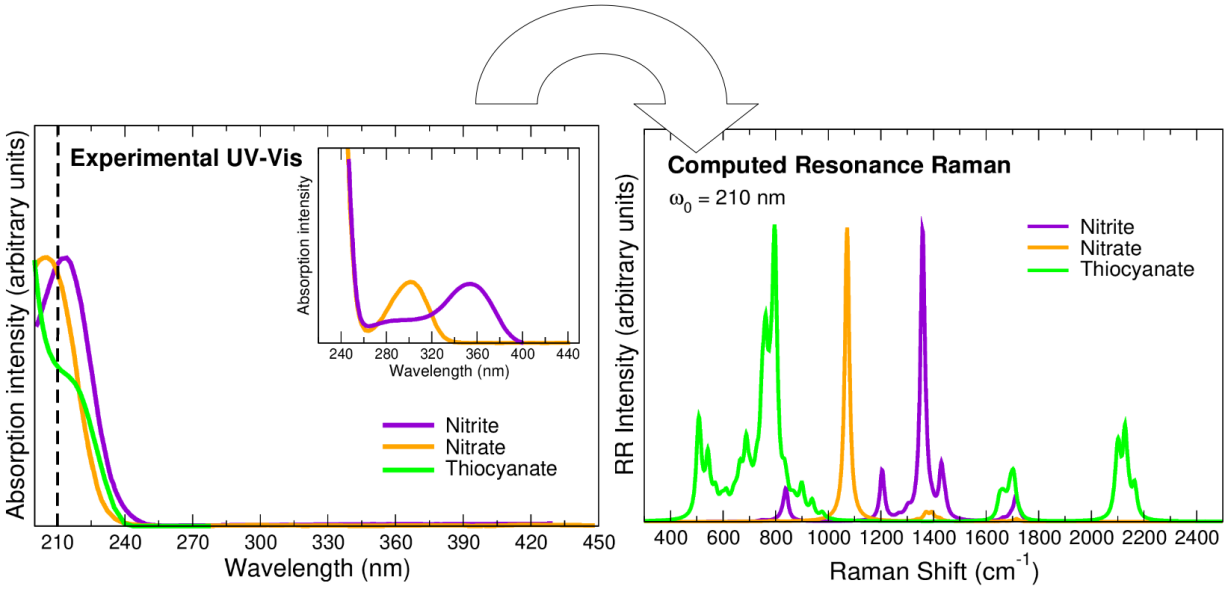
Experimental UV-Vis
Absorption intensity (arbitrary units)
Wavelength (nm)
210 240 270 300 330 360 390 420 450
Absorption intensity
Wavelength (nm)
240 280 320 360 400 440
Nitrite
Nitrate
Thiocyanate
Computed Resonance Raman
ω_0 = 210 nm
RR Intensity (arbitrary units)
Raman Shift (cm^{-1})
400 600 800 1000 1200 1400 1600 1800 2000 2200 2400
Nitrite
Nitrate
Thiocyanate

698